Petroleum Science 23 (2026) 5497–5508

Contents lists available at ScienceDirect

Petroleum Science

journal homepage: www.keaipublishing.com/en/journals/petroleum-science

Original Paper

In-situ anaerobic microbial oxidation of alkane gases within tight shale reservoir in the Ordos Basin: Evidence from intramolecular isotope compositions of desorbed propane

Rui-Liang Guo [a,b], Juske Horita [c], Ji-Hong Li [d], Yun-Chao Hou [d], Jun-Lin Chen [e], Peng Liu [f,*]

[a] School of Earth Sciences and Engineering, Xi'an Shiyou University, Xi'an, 710065, Shaanxi, China
[b] Shaanxi Key Laboratory of Petroleum Accumulation Geology, Xi'an Shiyou University, Xi'an, 710065, Shaanxi, China
[c] Department of Geosciences, Texas Tech University, Lubbock, 79409, TX, USA
[d] Exploration and Development Research Institute of PetroChina Changqing Oilfield Company, Xi'an, 710018, Shaanxi, China
[e] Key Laboratory of Petroleum Resources, Northwest Institute of Eco-Environment and Resources, Chinese Academy of Sciences, Lanzhou, 730000, Gansu, China
[f] College of Safety Science and Engineering, Xi'an University of Science and Technology, Xi'an, 710054, Shaanxi, China

ARTICLE INFO

Article history:
Received 31 October 2025
Received in revised form
5 January 2026
Accepted 24 March 2026
Available online 28 March 2026

Edited by Min Li

Keywords:
Microbial anaerobic oxidation
Propane
Position-specific carbon isotope
Chang 7 shale
The Ordos basin

ABSTRACT

Anaerobic microbial oxidation of hydrocarbons is a key biogeochemical process influencing hydrocarbon compositions and the carbon cycle in subsurface systems. In this study, the microbial oxidation of propane within the Chang 7 shale of the Ordos Basin was investigated through intramolecular carbon isotope analysis of thermally desorbed gases. The results show that samples affected by microbial activity exhibit elevated $\Delta_{C\text{-}T}$ values (3.9‰–7.9‰), $\delta^{13}C_{central}$ values ranging from −27.2‰ to −22.9‰, and $\delta^{13}C_{terminal}$ values from −31.1‰ to −30.5‰, significantly higher than non-degraded samples. These isotopic characteristics indicate that microorganisms preferentially oxidize the central carbon atom in propane, while the terminal carbon retains its original isotopic signature. The distinct position-specific isotopic patterns serve as sensitive indicators of microbial degradation in shale reservoirs. Furthermore, sedimentological data suggest that microbial degradation potential is closely linked to the sand supply from different sedimentary facies. Toward deeper lacustrine settings, reductions in sandy interlayer thickness and grain size, along with enhanced nanoconfinement effects, restrict nutrient diffusion and microbial mobility, resulting in limited degradation despite favorable thermal conditions. This study confirms that intramolecular-level isotopic techniques provide powerful tools for identifying microbial processes in low-permeability shales and contribute to a better understanding of shale oil and gas reservoir evolution.

1. Introduction

Anaerobic microbial oxidation of hydrocarbons plays a crucial role in the carbon cycle in the subsurface of the earth. Diverse forms of hydrocarbons have been discovered in the lithosphere, hydrosphere, atmosphere and the biosphere (Kniemeyer et al., 2007). The distributions of hydrocarbons within the earth are influenced by geological, chemical, and biological processes with significant spatial and genetic heterogeneity (Luo et al., 2020). Anaerobic microbial oxidation of hydrocarbons refers to the respiration process, by which microorganisms utilize electron acceptor other than O_2 for reduced carbon compounds to generate energy for their growth (Zengler et al., 1999; Widdel and Rabus, 2001; Pavlova et al., 2022; Dang et al., 2024). Alternative electron acceptors include sulfate (SO_4^{2-}), nitrate (NO_3^-), iron (Fe^{3+}), manganese (Mn^{4+}), or carbonate (CO_3^{2-}) to drive microbial metabolism (Heider et al., 1998).

Petroleum reservoirs are currently the most widely utilized and economically valuable forms of hydrocarbon accumulation. It has been confirmed that anaerobic microbial oxidation widely occurred in conventional petroleum reservoirs and the oil-water

* Corresponding author.
E-mail address: pengliu@xust.edu.cn (P. Liu).
Peer review under the responsibility of China University of Petroleum (Beijing).

https://doi.org/10.1016/j.petsci.2026.03.052

contact (OWC) is a dynamic zone where microbial activity can thrive due to the presence of water, electron acceptors, and nutrients (Meckenstock et al., 2014; Wang et al., 2019; Sierra-Garcia et al., 2020). Previously, anaerobic microbial oxidation of hydrocarbons in conventional petroleum systems from different sedimentary basins has been identified (Gao et al., 2013; Pavlova et al., 2022; Kim et al., 2023). Shale oil and gas acts as an important unconventional petroleum system and it is characterized by self-generation, self-storage, and in-situ accumulation (Guo et al., 2022; Song et al., 2025). Generally, Shale reservoirs, characterized by their tight lithology and low porosity and permeability, exhibit severely restricted nutrient diffusion and microbial motility (Shen et al., 2018; Ding et al., 2023; Zeng et al., 2023). Even under thermally favorable conditions (<80 °C), these reservoirs are generally considered unfavorable for microbial anaerobic oxidation of hydrocarbons due to the limited mass transfer capabilities and spatial constraints that impede microbial metabolic processes (Gittins et al., 2023; McIntosh et al., 2023). The nano-scale pore throat architecture creates substantial mass transfer barriers, effectively inhibiting both nutrient replenishment and microbial colonization required for sustaining anaerobic oxidation pathways (Yao et al., 2019). However, previous studies have documented pronounced microbial anaerobic oxidation at the contact interface between the Chang 7 (Ch-7) shale and adjacent sandstone intervals, the desorbed hydrocarbon gases of the shale within the contact interface exhibit obviously larger $\delta^{13}C$ values and this is attributed to localized biogeochemical activity facilitated by enhanced fluid migration pathways and microscale geochemical gradients at lithological boundaries (Meng et al., 2017).

In shale oil and gas systems, in-situ microbial oxidation can substantially affect the mobility of retained shale oil and the gas-bearing capacity of shale reservoirs. However, this process remains poorly understood due to the lack of effective methods for its precise identification. Carbon isotopic signatures of hydrocarbons are widely applied in identifying microbial anaerobic oxidation. In general, the $\delta^{13}C$ values of residual hydrocarbons increase with increasing microbial anaerobic oxidation (Whiticar and Faber, 1986). The preferential oxidation of hydrocarbons by microorganism in the order $C_3 > nC_4 > nC_5 > iC_5 > iC_4 > >$ neoC_5 (Head et al., 2003; Martini et al., 2008). Hence, $\delta^{13}C_3$ values are a relatively sensitive indicator for microorganism oxidation. However, the compound-specific isotopic signatures of anaerobic oxidation can be identified only at high microbial oxidation levels associated with large consumptions of propane (Jaekel et al., 2013; Meng et al., 2017). Recent advances in intramolecular carbon isotope of propane provide a sensitive means to detect even subtle anaerobic microbial oxidation within low-permeability shale matrices. During propane oxidized by microorganisms, the central carbon atom within propane molecule is preferentially activated by addition of radicals to fumarate, leading to different carbon isotopic fractionation factors at the different positions (Jaekel et al., 2014; Gilbert et al., 2019). Previous study revealed that the $\delta^{13}C$ values of the central carbon (–CH_2–) of propane significantly increase with extent of oxidation by microorganisms, while the terminal carbon (–CH_3) remains almost constant (Wang et al., 2024). Therefore, the $\delta^{13}C$ values of the central carbon of propane could provide us a sensitive indicator for reflecting microbial anaerobic oxidation in natural gas reservoirs.

In this study, the hydrocarbons within the shale from Yanchang Formation of the Ordos Basin were extracted by the thermal desorption apparatus, the thermally desorbed hydrocarbons were determined and the intramolecular carbon isotopic compositions of propane were measured by a q-NMR calibrated GC-Py-GC-IRMS method. The results demonstrate in-situ microbial anaerobic oxidation of hydrocarbons in the matrix of low-permeability shale, substantiating previously unrecognized anaerobic oxidation potential under nano-confined conditions.

2. Geological setting

The Ordos Basin, a Late Triassic lacustrine foreland basin, is structurally subdivided into six tectonic units: the Weibei uplift, the Yishan slope, the Yimeng uplift, the Jinxi flexure belt, the Western thrust belt, and the Tianhuan depression (Guo et al., 2024) (Fig. 1(a)). During the Late Triassic, the basin underwent a transition from a marginal marine to a fully continental lacustrine depositional system, leading to the accumulation of the Yanchang Formation. This formation comprises a suite of fluvial, lacustrine, and deltaic clastic deposits interbedded with volcanic tuff layers, mudrocks, siltstones, and sandstones.

The Yanchang Formation is stratigraphically divided into ten members from the Ch-10 at the bottom to the Ch-1 at the top (Fig. 1(b)). Among these, the Ch-7 sub-member represents the peak of lacustrine development, characterized by extensive deposition of organic-rich mudrocks that created favorable conditions for shale oil accumulation. The thickness of the Ch-7 interval ranges between 100 and 120 m with fine sandstone, sandy mudstone, and organic-rich mudrocks accounting for approximately 21%, 54%, and 25% of the total lithology, respectively (Changqing Oilfield Company). The elevated total organic carbon (TOC) content within the Ch-7 member (5.21% in average) is considered a principal factor controlling the shale oil potential in the Ordos Basin, positioning it as a key target for hydrocarbon exploration and development (Guo et al., 2025b).

3. Samples and methods

3.1. Samples

Five Ch-7 shale samples were collected across the southwestern to northeastern regions of the basin, covering the transition from semi-deep lacustrine to deep lacustrine facies with depths ranging from 1622.62 to 1693.50 m. The exact well locations are shown in Fig. 1(a). The basic geochemical characteristics of the samples were obtained from the Changqing Oilfield Exploration and Development Research Institute to clarify the kerogen classification and assess their hydrocarbon generation potential.

3.2. Methods

3.2.1. Extraction of residual hydrocarbons within shale

In this study, residual hydrocarbons adsorbed within the shale matrices were extracted via thermal desorption, utilizing an apparatus previously described by Liu et al. (2025) (Fig. 2). The system is composed of three main components: a purge control module, a thermal desorption assembly, and an analytical detection unit. The purge system employed ultra-high purity argon (99.999%) regulated by an AST10 mass flow controller (Asert Instrument, Beijing). The desorption apparatus includes a programmable pyrolysis furnace (Hefei Kejing Materials Technology), quartz tubing, dual 2-way needle valves, and a pressure gauge rated for 0–2 MPa. The detection module features a 6-port switching valve coupled to a FULI 9790 Plus gas chromatograph (Zhejiang Fuli Analytical Instruments) equipped with a flame ionization detector (FID).

Powdered shale samples (sieved to 20–60 mesh) were placed in the middle of the quartz tube, flanked by quartz rods to reduce dead volume. The system was purged with argon for 10 min to displace atmospheric gases. After closing the valves (A and B), the samples were heated at a rate of 20 °C/min to 180 °C and

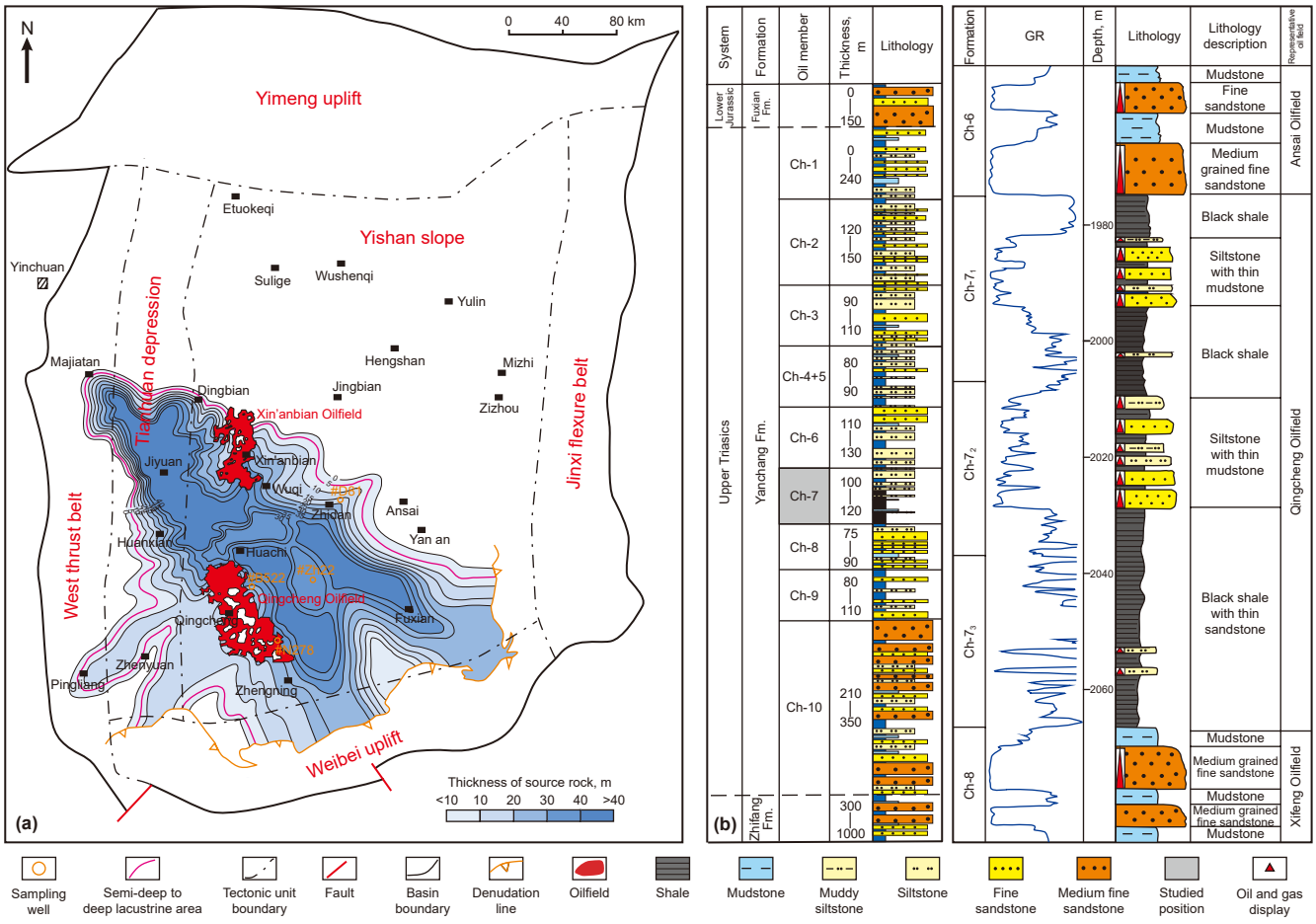

Fig. 1. (**a**) Tectonic framework and (**b**) stratigraphic overview of the Ordos Basin and Yanchang Formation.

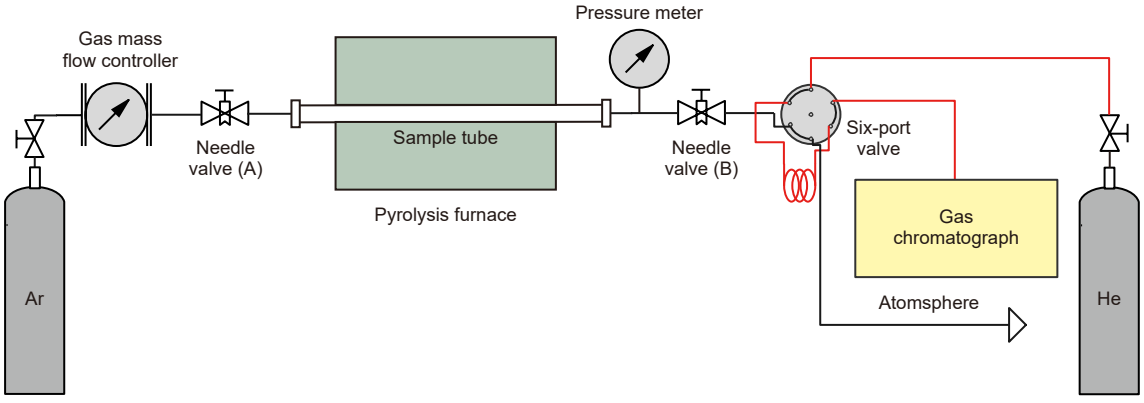

Fig. 2. Schematic diagram of the thermal desorption apparatus (Liu et al., 2025).

maintained isothermally for 60 min. Hydrocarbon desorption during the heating led to a gradual pressure increase within the system. Upon completion, valve B was opened, allowing the evolved gases to be introduced into the chromatograph for analysis.

All operational parameters, including the gas flow, furnace heating profile, and chromatographic temperature programming, were software-controlled. Chromatographic separation was achieved using an HP-PONA column (50 m × 0.20 mm i.d.) with an initial hold at 40 °C for 2 min, followed by a ramp to 100 °C at 2 °C/min, and then to 260 °C with a 20-min hold. Relative abundances of C_1–C_{14} hydrocarbons was quantified, and the evolved gases were concurrently collected in an inverted container immersed in saturated NaCl solution for isotopic analyses.

3.2.2. Compound-specific carbon isotope composition

The compound-specific carbon isotopic composition of the thermally released hydrocarbon gases was measured using a Thermo Scientific 253 Plus isotope ratio mass spectrometer (IRMS) interfaced with a Thermo Scientific Trace 1310 gas chromatograph. Separation was performed using a 30 m × 0.32 mm i.d. HP-PLOT Q

capillary column. The GC oven program began with an isothermal hold at 30 °C for 10 min, followed by a temperature ramp of 20 °C/min to 180 °C, where it was held for an additional 2 min. Carbon isotope ratios ($\delta^{13}C$) were expressed relative to the Vienna Pee Dee Belemnite (V-PDB) standard with an analytical precision of ±0.5‰.

3.2.3. Intramolecular carbon isotope determination of propane

The measurements of intramolecular carbon isotope distributions of thermally desorbed propane were conducted using a quantitative (q) NMR-calibrated GC-Py-GC-IRMS protocol, as detailed in our earlier publications (Liu et al., 2023a, 2023b, 2024; Wang et al., 2024).

The previous research has demonstrated that propane pyrolysis products follow distinct molecular formation pathways (Gilbert et al., 2016). The position-specific carbon isotope values—$\Delta_{C\text{-}T}$ ($\delta^{13}C_{central}$–$\delta^{13}C_{terminal}$), $\delta^{13}C_{central}$, and $\delta^{13}C_{terminal}$—were calculated using the following equations:

$$\Delta_{C\text{-}T}\ (‰) = 2 \times \delta^{13}C_{ethylene} - 2 \times \left(\delta^{13}C_{methane} \times S_{methane} + \delta^{13}C_{ethane} \times S_{ethane}\right) \Big/ \left(S_{methane} + S_{ethane}\right) \quad (1)$$

$$\delta^{13}C_{central}\ (‰) = \left(3 \times \delta^{13}C_{propane} + 2 \times \Delta_{C\text{-}T}\right) \Big/ 3 \quad (2)$$

$$\delta^{13}C_{terminal}\ (‰) = \left(3 \times \delta^{13}C_{propane} - \Delta_{C\text{-}T}\right) \Big/ 3 \quad (3)$$

where, $S_{methane}$ and S_{ethane} denote the signal intensities of CO_2 generated during $\delta^{13}C$ measurements of methane (C_1) and ethane (C_2), respectively.

Liu et al. (2023a) compared $\Delta_{C\text{-}T}$, $\delta^{13}C_{central}$, and $\delta^{13}C_{terminal}$ values derived from the quantitative ^{13}C NMR and the GC-Py-GC-IRMS approaches. Their findings indicated constant intramolecular carbon fractionation patterns during the propane pyrolysis, relative to the q-NMR results. Accordingly, position-specific isotope correction factors established for the GC-Py-GC-IRMS system were adopted in this study to ensure accurate quantification of the $\Delta_{C\text{-}T}$, $\delta^{13}C_{central}$, and $\delta^{13}C_{terminal}$ parameters.

4. Results

4.1. Chemical compositions of light hydrocarbons (C_1–C_{14}) within shale

Distributions of light hydrocarbons (C_1–C_{14}) extracted from the Ch-7 shale samples were shown in Fig. 3 and Table 1. Generally, propane was the main peak of the gas chromatograms of extracted hydrocarbons in shale samples N278-1 and N278-2. In addition, *n*-alkanes exhibit higher concentrations than iso-alkanes, naphthenes, and aromatics of the same carbon number. However, in the thermally desorbed hydrocarbons of the three other samples (D81, B522 and Zh22), methylcyclohexane occurs at higher concentrations and dominates as the principal peak among C_7–C_{14} hydrocarbons. Remarkably, in sample D81, methylcyclohexane exceeds the cumulative abundance of C_1–C_6 compounds, establishing itself as the dominant peak across the entire C_1–C_{14} light hydrocarbon range. This differential pattern provides a geochemical signature of post-generation processes. Therefore, the light hydrocarbon (C_1–C_{14}) components are not useful for discriminating source rock organic matter types and thermal maturity levels. The geochemical evidence of post-generation processes revealed by light hydrocarbons will be comprehensively addressed in the discussion section.

4.2. Inter- and intra-molecular isotopic compositions of thermally desorbed propane

Liu et al. (2025) indicates that distinct chemical compositional fractionation and isotopic fractionation of C_{1-2} hydrocarbons in thermally desorbed gases have been demonstrated. Concurrently, the isotopic fractionation characteristics between the free and adsorbed states of C_{1-2} hydrocarbons within shales are closely associated with the adsorption ratio and pore-size distribution (Liu et al., 2020). Hence, this study focuses exclusively on the C_3 for detailed discussion. Bulk and position-specific isotopic composition of propane in thermally desorbed hydrocarbons within shale samples were presented in Table 2. In general, the bulk and position-specific isotopic composition of thermally desorbed propane can be divided into two groups (Fig. 4). Thermally desorbed propane from shale samples of well N278 have lower $\delta^{13}C_3$ values with an average of −34.4‰, while thermally desorbed propane from shale samples of wells D81, B522 and Zh22 have higher $\delta^{13}C_3$ values with ranging from −29.8‰ to −28.2‰ (average: −29.0‰). In addition, average $\Delta_{C\text{-}T}$ values of thermally desorbed propane from shale samples of well N278 is 3.0‰. However, $\Delta_{C\text{-}T}$ values of thermally desorbed propane from shale samples of wells D81, B522 and Zh22 range from 3.9‰ to 7.9‰ with an average of 5.4‰. Meanwhile, the $\delta^{13}C_{central}$ and $\delta^{13}C_{terminal}$ values of these two groups are characterized by distinct distributions. The average $\delta^{13}C_{central}$ and $\delta^{13}C_{terminal}$ values thermally desorbed propane from shale samples of well N278 are −32.4‰ and −35.4‰, respectively. However, the $\delta^{13}C_{central}$ values thermally desorbed propane from shale samples of wells D81, B522 and Zh22 are characterized by wide distributions with ranging from −27.2‰ to −22.9‰, while the $\delta^{13}C_{terminal}$ values thermally desorbed propane from above shale samples are relatively stable with ranging from −31.1‰ to −30.5‰. Generally, the $\delta^{13}C_{central}$ and $\delta^{13}C_{terminal}$ values of thermally desorbed propane from shale samples of wells D81, B522 and Zh22 is larger than those of well N278.

5. Discussion

5.1. Position-specific isotope fractionation of propane

Shale oil and gas are important unconventional resources characterized by self-generation and self-storage within low-permeability systems (Guo et al., 2022). In general, petroleum within shale exists as varying states, including adsorbed states in the matrix and free states in pores and cracks (Guo et al., 2022). Previous studies confirmed that stable isotope fractionation of methane and ethane occurs in adsorption/desorption processes (Liu et al., 2020; Wang et al., 2022). However, bulk carbon isotope compositions of propane in hydrocarbons desorbed from Ch-7 shale core samples of the Ordos Basin reveal that no obvious carbon isotope fractionation can be observed in desorption of hydrocarbons within shale, suggesting bulk isotope compositions of propane can remain relatively constant during adsorption/desorption processes. Guo et al. (2025a) measured the position-specific isotopic compositions of the propane in associated gases of Ch-7 shale oil in the Ordos Basin, and their position-specific isotopic results are compared with the thermally desorbed propane within shale of this study (Figs. 5 and 6). Figs. 5 and 6 show that the bulk and position-specific isotopic compositions of associated propane in shale oil fall in the same range of those of the thermally desorbed propane in the well N278. The well N278 is in the shale oil production area (Fig. 1(a)) and the results further confirmed that adsorption/desorption does not lead to obvious position-specific isotopic fractionation of propane.

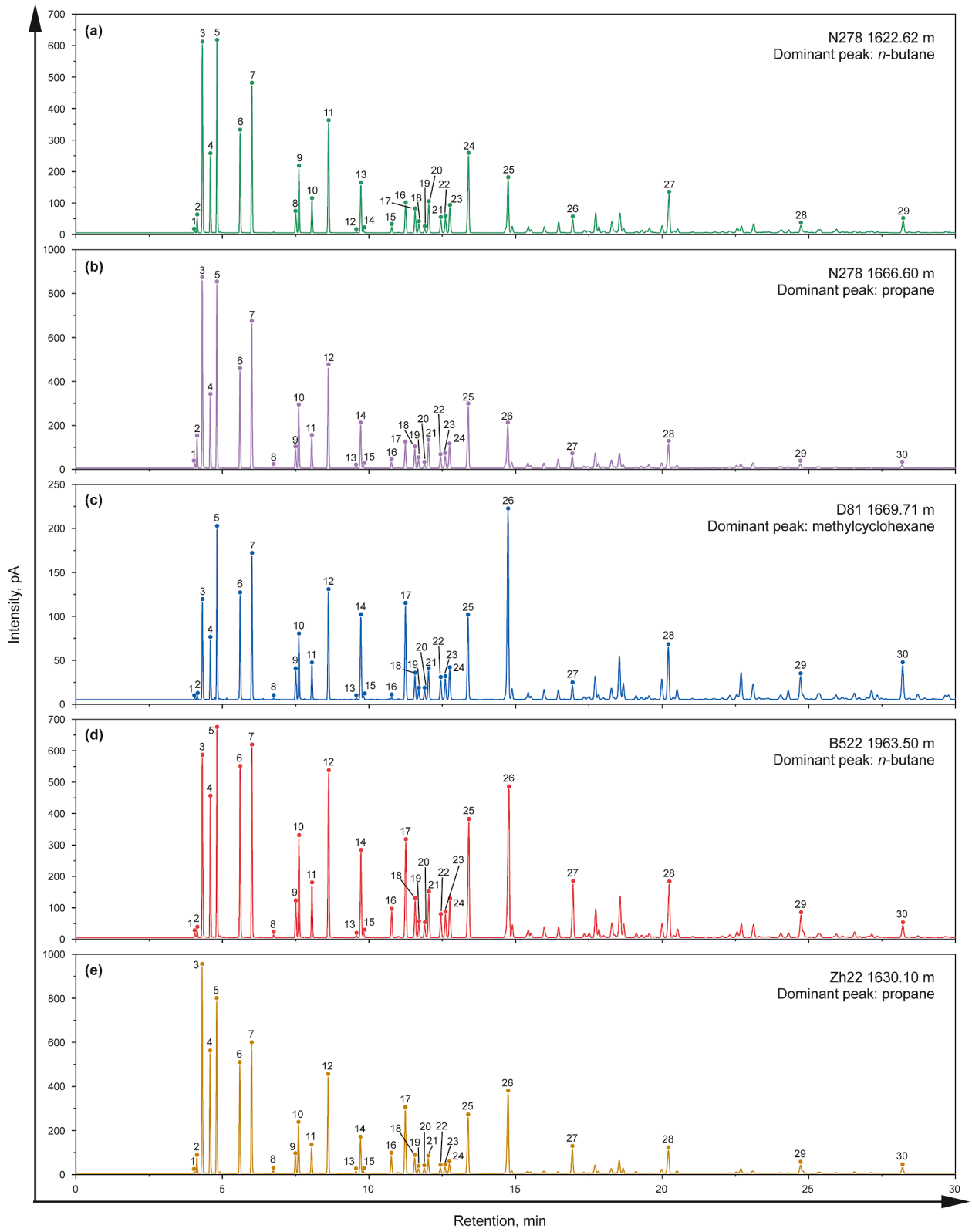

Fig. 3. Distributions of light hydrocarbons (C_1–C_{14}) desorbed from the Ch-7 shale.

The differences in the bulk and position-specific isotopic compositions of associated propane in shale oil and thermally desorbed propane in the wells D81, B522 and Zh22 may be due to their different maturation stages and kerogen structures. Previous studies indicate that the vitrinite reflectance (R_o) of the Ch-7 shale in the study area ranges from 0.8% to 1.0% (Guo et al., 2022), suggesting that the shale samples from different wells are likely within a comparable thermal maturity stage. Hence, larger bulk

Table 1
Lookup table of light hydrocarbon compound names in Fig. 3.

No.	Name	No.	Name
1	Methane	16	Benzene
2	Ethane	17	Cyclohexane
3	Propane	18	2-Methylhexane
4	Isobutane	19	2,3-Dimethylpentane
5	*n*-Butane	20	1,1-Dimethylpentane
6	Isopentane	21	3-Methylhexane
7	*n*-Pentane	22	cis-1,3-Dimethylcyclopentane
8	2,2-Dimethylbutane	23	trans-1,3-Dimethylcyclopentane
9	2,3-Dimethylbutane	24	trans-1,2-Dimethylcyclopentane
10	2-Methylpentane	25	*n*-Heptane
11	3-Methylpentane	26	Methylcyclohexane
12	*n*-Hexane	27	Toluene
13	2,2-Dimethylpentane	28	*n*-Octane
14	Methylcyclopentane	29	Dimethylbenzene
15	2,4-Dimethylpentane	30	*n*-Nonane

and position-specific isotopic compositions of the thermally desorbed propane from the wells D81, B522 and Zh22 likely reflect a higher contribution of terrestrial plant-derived Type III kerogen, while N278-1 and N278-2 are likely characterized by type I/II kerogen.

In addition, two different carbon positions within propane, primary carbon in the terminal positions and secondary carbon in the central position, are characterized by different reactive potentials in chemical and bio-chemical processes. The central carbon of propane is more reactive in radical reactions because the radical formed at this position is stabilized by hyperconjugation, making it easier to break the C–H bond compared to the terminal carbons (Wang et al., 2024). Previous studies revealed that the central carbon of propane exhibits preferential reactivity in both chemical and bio-chemical processes, resulting in significant ^{13}C enrichments at the central carbon position at remaining propane, whereas the terminal carbons display minimal isotopic fractionation (Wang et al., 2024; Liu et al., 2025). Consequently, the terminal carbons of propane preserve the primary isotopic signatures inherited during propane formation, serving as a novel isotopic indicator for tracing hydrocarbon origins (Liu et al., 2024, 2025). Fig. 7 shows the relationship between $\delta^{13}C_{terminal}$ and $\delta^{13}C_3$ values of natural propane of coal-type and oil-type natural gases from different basins. The results indicate that the bulk and position-specific isotopic compositions of the thermally desorbed propane in this study fall within the oil-type natural gas. However, the data of the thermally desorbed propane from the wells D81, B522 and Zh22 demonstrates that their bulk and position-specific isotopic compositions are more consistent with coal-type natural gas in contrast to the thermally desorbed propane from the well N278, suggesting that higher plants contributed to the organic matter in shale from the wells D81, B522 and Zh22, compared to that from the well N278.

5.2. In-situ anaerobic microbial oxidation of propane within tight shale

The relationship of $\delta^{13}C_{central}$ and $\delta^{13}C_{terminal}$ values of propane in shale samples and oil-type natural gas reservoirs from different basins are shown in Fig. 8. A large majority of the data exhibit trends that are consistent with Rayleigh-type fractionation models during the thermal cracking of sapropelic kerogen from the *n*-propyl pathway (Liu et al., 2024). In contrast, the intramolecular isotope reversal ($C_{central} < C_{terminal}$) observed in propane from the Santanghu Basin has been demonstrated to be associated with a rapid shift in the propane formation pathway during the early stages of thermal maturation (Liu et al., 2024). The position-specific isotopic composition of thermally desorbed propane from the Ch-7 shale shows that thermally desorbed propane

Table 2
Bulk and position-specific isotopic composition of propane in thermally desorbed hydrocarbons within Ch-7 shale from the Ordos Basin.

Samples	Depth, m	Gas composition, %	Compound-specific carbon isotopic composition, ‰	Position-specific carbon isotopic composition, ‰		
		C_3H_8	C_3H_8	Δ_{C-T}	$\delta^{13}C_{central}$	$\delta^{13}C_{terminal}$
N278-1	1622.62	0.48	−35.1	3.5	−32.8	−36.3
N278-2	1666.60	0.68	−33.7	2.5	−32.0	−34.5
D81	1669.71	0.08	−29.8	3.9	−27.2	−31.1
B522	1963.50	0.46	−29.0	4.4	−26.0	−30.5
Zh22	1630.10	0.75	−28.2	7.9	−22.9	−30.8

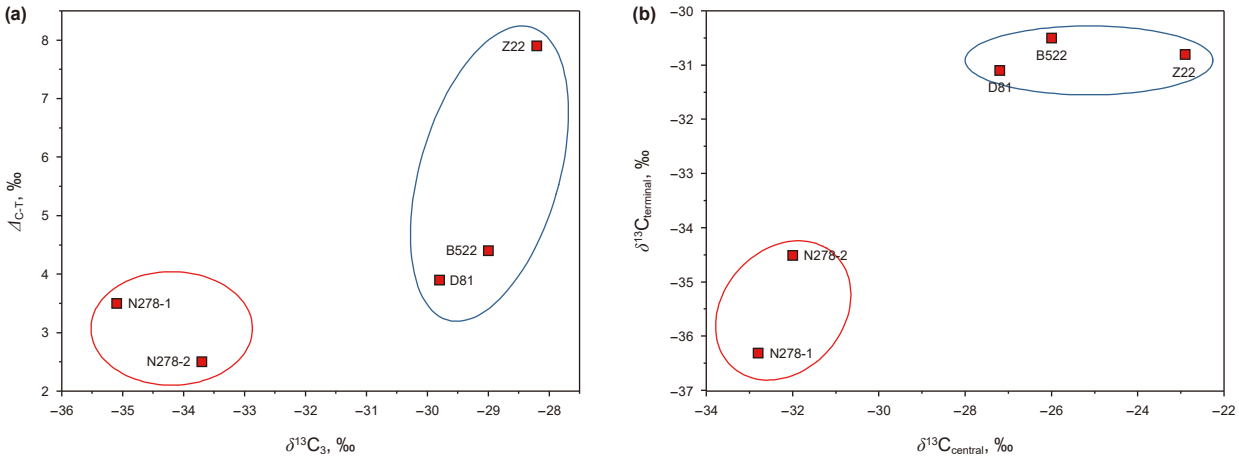

Fig. 4. Δ_{C-T} vs. $\delta^{13}C_3$ (**a**) and $\delta^{13}C_{central}$ vs. $\delta^{13}C_{terminal}$ (**b**) of thermally desorbed propane extracted from Ch-7 shale of the Ordos Basin.

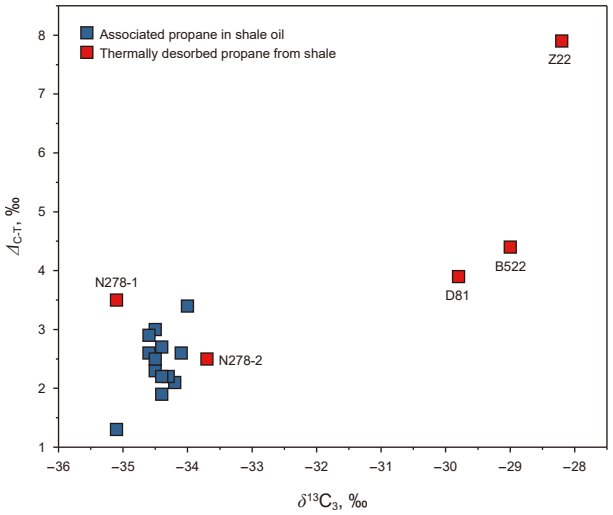

Fig. 5. Relationship of Δ_{C-T} and $\delta^{13}C_3$ values of propane from thermally desorbed hydrocarbons from shale (this study) and associated natural gases in shale oil (Guo et al., 2025a) of the Ordos Basin.

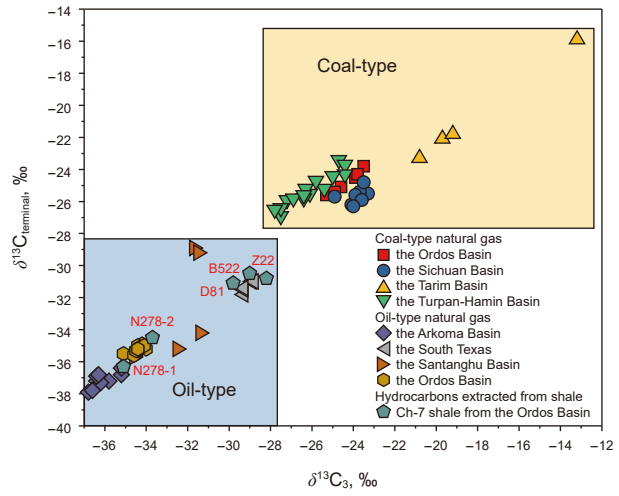

Fig. 7. Relationship between $\delta^{13}C_{terminal}$ and $\delta^{13}C_3$ values of natural propane of coal-type and oil type natural gases from different basins. The data of coal-type natural gas from the Ordos Basin (Wang et al., 2024), Sichuan Basin (Liu et al., 2023b), Tarim Basin and Turpan-Hami Basin (Liu et al., 2024). The data of oil-type natural gas from the Arkoma Basin (Liu et al., 2018), South Texas (Zhao et al., 2020), Santanghu Basin (Liu et al., 2024) and the Ordos Basin (Liu et al., 2025).

samples from the well N278 are characterized by similar position-specific isotopic distributions compared to propane in the associated gases of Ch-7 shale oil of the Ordos Basin and the Woodford shale gas of the Arkoma Basin. In addition, thermally desorbed propane from the well N278 and associated propane of Ch-7 shale oil of the Ordos Basin fit well with results from the anhydrous pyrolysis of Woodford shale (Type II kerogen) at low maturity level with an Easy R_o of 0.76%. Previously, it has been confirmed that the Ch-7 shale of the Ordos Basin has R_o ranging from 0.8% to 1.1% at early maturation stage (Guo et al., 2022). Moreover, thermally desorbed propane from wells D81, B522, and Zh22, as well as propane from the Eagle Ford shale gas in South Texas, is consistent with the experimental results of anhydrous pyrolysis of the Woodford Shale at high temperatures. However, Previous studies indicate that the Eagle Ford shale gas in South Texas has higher source-rock R_o values (1.1%–1.2%) than the Ch-7 shale samples (0.8%–1.1%) (Zhang et al., 2017; Guo et al., 2022). The discrepancies observed between the experimental and simulation results suggest that the organic matter in the Eagle Ford shale in the South Texas and Ch-7 shale from the wells D81, B522 and Zh22 has a greater contribution from higher plant sources.

However, notable differences exist among the position-specific isotopic composition of propane in the Eagle Ford shale gas and extracted hydrocarbons in the Ch-7 shale from the wells D81, B522 and Zh22. For Eagle Ford shale gas, the position-specific isotope compositions of propane remain relatively stable. Whereas, compared to the relative stable $\delta^{13}C_{terminal}$ values of the thermally desorbed propane from shale from the wells D81, B522 and Zh22, the $\delta^{13}C_{central}$ values of the samples are widely distributed with ranging from −27.2‰ to −22.9‰, revealing that the propane within the shale samples could altered by irreversible kinetic post-generation processes involved in chemical and bio-chemical reactions.

It has been previously confirmed that various post-generation processes, including thermochemical sulfate reduction (TSR) and microbial anaerobic oxidation, exhibit a preferential reactivity toward the central carbon atom of propane (Liu et al., 2025). Previous study reveals that Δ_{C-T} and $\delta^{13}C_{central}$ values of propane in TSR altered natural gas samples from the Ordos Basin increase with increasing TSR alteration (Liu et al., 2026). In contrast, $\delta^{13}C_{terminal}$ values of propane remain largely unaltered by TSR reaction (Liu

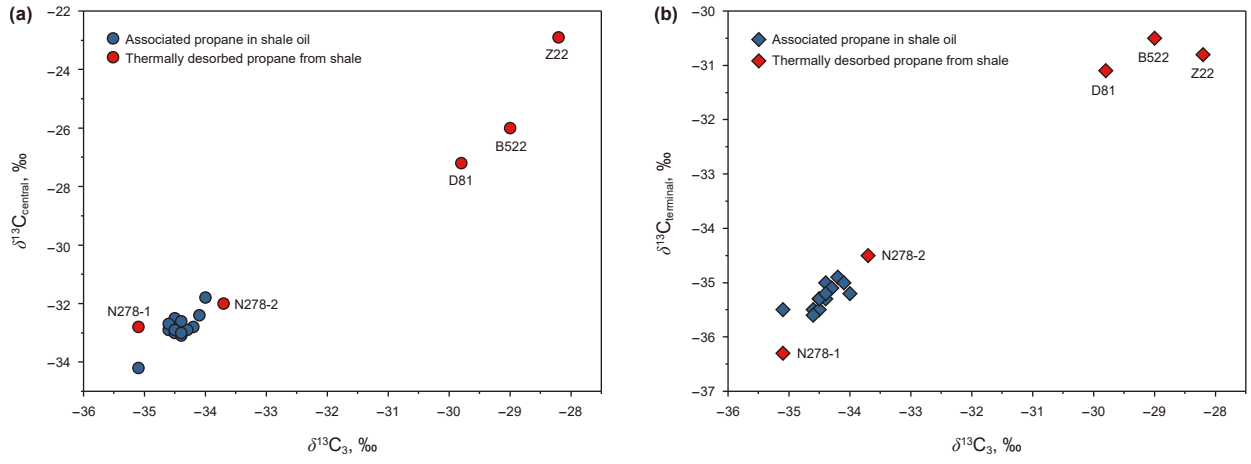

Fig. 6. Relationship of carbon isotopic compositions at (**a**) the central position, (**b**) the terminal position vs. $\delta^{13}C_3$ values of propane from thermally desorbed hydrocarbons from shale (this study) and associated natural gases in shale oil (Guo et al., 2025a) of the Ordos Basin.

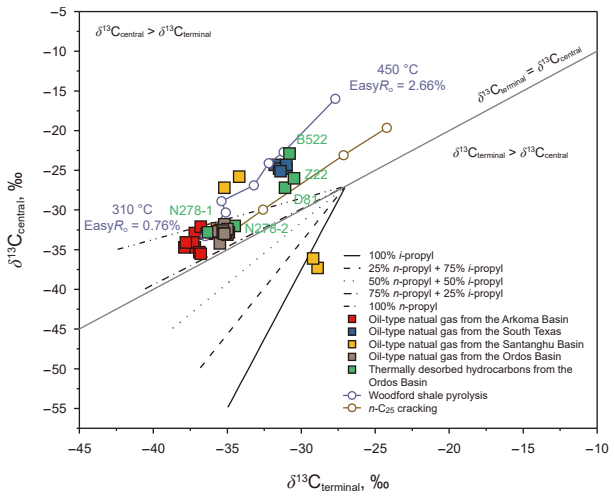

Fig. 8. Relationship between $\delta^{13}C_{central}$ and $\delta^{13}C_{terminal}$ values of natural propane with different formation process. The data of the Arkoma Basin (Liu et al., 2018), South Texas Basin (Zhao et al., 2020), Sangtanghu Basin (Liu et al., 2024) and the Ordos Basin (Guo et al., 2025a). The $\delta^{13}C$ value of the kerogen was assumed to be −27.0‰ in the original material followed by Whiticar (1996). Data from Woodford shale pyrolysis (Li and Horita, 2022) and n-C_{25} cracking (Gilbert et al., 2019).

et al., 2025). However, TSR typically occurs under high-temperature conditions (120–200 °C) and requires sulfate minerals (e.g., gypsum or anhydrite) as reactants (Jiang et al., 2014; Zhao et al., 2020). The burial depth of the Ch-7 shale samples is less than 2000 m, with temperatures of ~70–80 °C, which are well below the threshold for TSR but still within the temperature range reported for anaerobic microbial activity in subsurface environments (Karnachuk et al., 2021).

Apart from TSR, anaerobic microbial oxidation of hydrocarbons is widely identified in subsurface natural gas reservoirs (Gilbert et al., 2019). The anaerobic microbial oxidation process of natural gas refers to the process, in which microorganisms utilize alkanes as an electron donor to oxidize alkanes to carbon dioxide or other intermediate products under anoxic conditions (Suarez-Zuluaga et al., 2015). The intermediate products are further oxidized to carbon dioxide or other small organic molecules. Previously, the compound-specific isotopic compositions of natural gas are applied in identifying anaerobic microbial oxidation process, and propane is preferentially oxidized by microorganisms among the alkane gases (Meng et al., 2017). Generally, $\delta^{13}C$ values of the residual alkanes increase with increasing anaerobic microbial oxidation of natural gases. Jaekel et al. (2014) and Gilbert et al. (2019) conducted experiments of anaerobic degradation of propane by marine sulfate-reducing bacteria, and the results indicate that the central carbon is preferentially attacked over the terminal carbon during anaerobic microbial oxidation process. Based on this finding, Wang et al. (2024) established an approach for identifying anaerobic microbial oxidation of propane. The slope of linear fitting of $\delta^{13}C_{central}$ and bulk $\delta^{13}C$ values of propane ($\varepsilon_{central}/\varepsilon_{bulk}$) produced by marine sulfate-reducing bacteria (BuS5) is 2.58, whereas the slope of linear fitting of $\delta^{13}C_{terminal}$ and bulk $\delta^{13}C$ of propane ($\varepsilon_{terminal}/\varepsilon_{bulk}$) is 0.22 (Fig. 9). The slope of linear fitting of $\delta^{13}C_{central}$ and bulk $\delta^{13}C$ of propane ($\varepsilon_{central}/\varepsilon_{bulk}$) from the pyrolysis of Woodford shale is 1.67, whereas the slope of linear fitting of $\delta^{13}C_{terminal}$ and bulk $\delta^{13}C$ of propane ($\varepsilon_{terminal}/\varepsilon_{bulk}$) is 0.76. Fig. 9 shows the linear relationships of position-specific isotopic and bulk isotopic compositions of propane from different sources in the Ordos Basin. The data of the associated propane from shale oil fit well with the Woodford shale pyrolysis results for both central and terminal carbon positions. While the data of the thermally desorbed propane from shale fits well with the experimental results of microbial anaerobic oxidation of propane for both central and terminal carbon positions, revealing that the widely varying $\delta^{13}C_{central}$ values of the thermally desorbed propane are very likely caused by microbial anaerobic oxidation process. In addition, microbial biodegradation preferentially depletes n-alkanes, followed by branched alkanes, thereby progressively enriching naphthenic compounds with increasing biodegradation intensity. Fig. 10(a) shows the relationship between nC_6/MCC_5 and nC_7/MCC_6. Generally, N278-1 and N278-2 have higher nC_6/MCC_5 and nC_7/MCC_6 ratios than those from other samples, showing that microbial biodegradation occurred in samples D81, B522 and Zh22. As microbial biodegradation intensifies, both the Benz/nC_6 and Tol/nC_7 ratios exhibit systematic increases. Samples B522 and Zh22 display markedly elevated Benz/nC_6 and Tol/nC_7 ratios relative to other samples (Fig. 10(b)). In contrast, sample D81 shows Benz/nC_6 and Tol/nC_7 values comparable to those of N278-1 and N278-2. This geochemical signature indicates that D81 has likely experienced evaporation fractionation, a process that preferentially enriches aromatic compounds relative to n-alkanes within the light hydrocarbon fraction. Accordingly, non-degraded samples in this study are defined as shale samples showing no evidence of microbial alteration, characterized by low and narrowly distributed

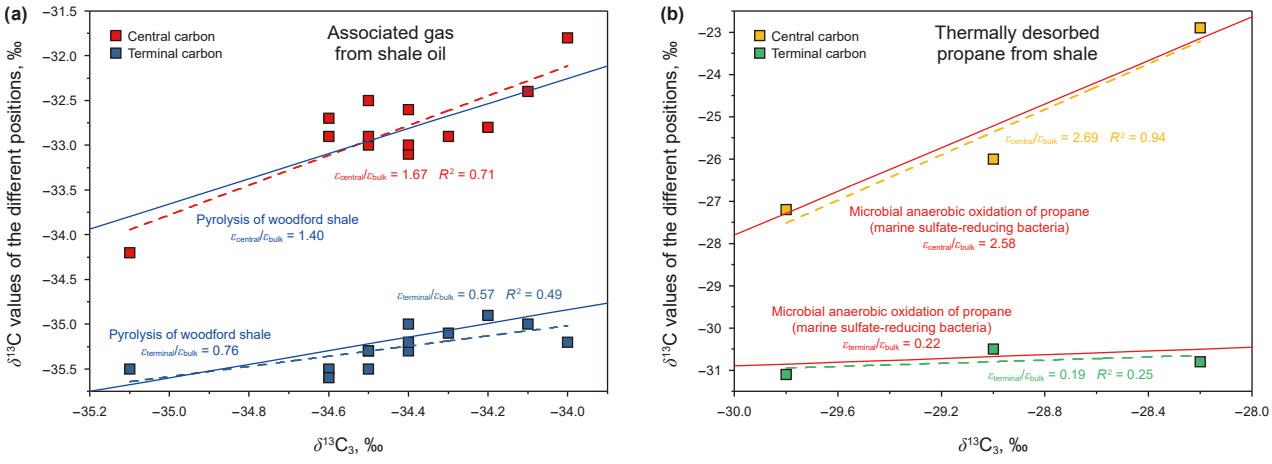

Fig. 9. Relationships between $\delta^{13}C$ and $\delta^{13}C$ values of the different positions: (**a**) associated gas from shale oil (Guo et al., 2025a) and (**b**) thermally desorbed gases of wells D81, B522 and Zh22 (this study) from the Ordos Basin.

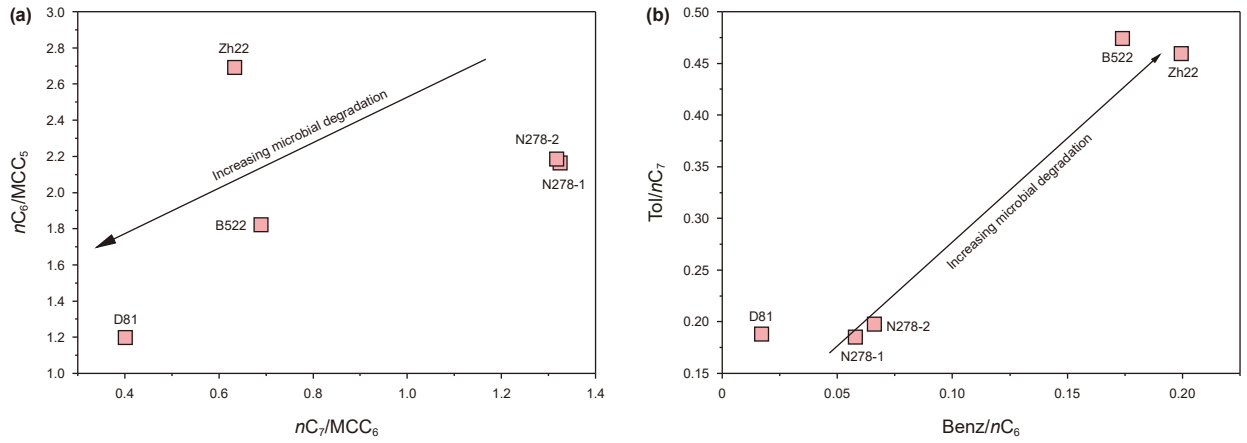

Fig. 10. nC_6/MCC_5 vs. nC_7/MCC_6 (**a**) and Benz/nC_6 vs. Tol/nC_7 (**b**) of extracted hydrocarbons from shale.

$\Delta_{C\text{-}T}$ values (approximately 2.5‰–3.5‰), which are comparable to associated gases from shale oil and consistent with primary thermogenic propane signatures.

5.3. Mechanism of microbial oxidation process in shallow shale

The anaerobic microbial oxidation within the Ch-7 shale is closely associated with its sedimentary evolution. During the deposition of the Middle Triassic Yanchang Formation, a large NW–SE-trending lacustrine basin developed, with the Ch-7 member representing the maximum lake transgression. Sediment supply was dominated by deep-water gravity flows derived from both southwestern and northeastern sources (Fig. 11) (Wang et al., 2021; Lyu et al., 2022). Under volcanic, seismic, and storm influences, slope failures generated sandy debris flows that evolved downslope into turbidity currents. These flows deposited sandy gravity-flow facies in the slope-to-basin transition zone, grading into laminated and finally homogeneous mudrocks

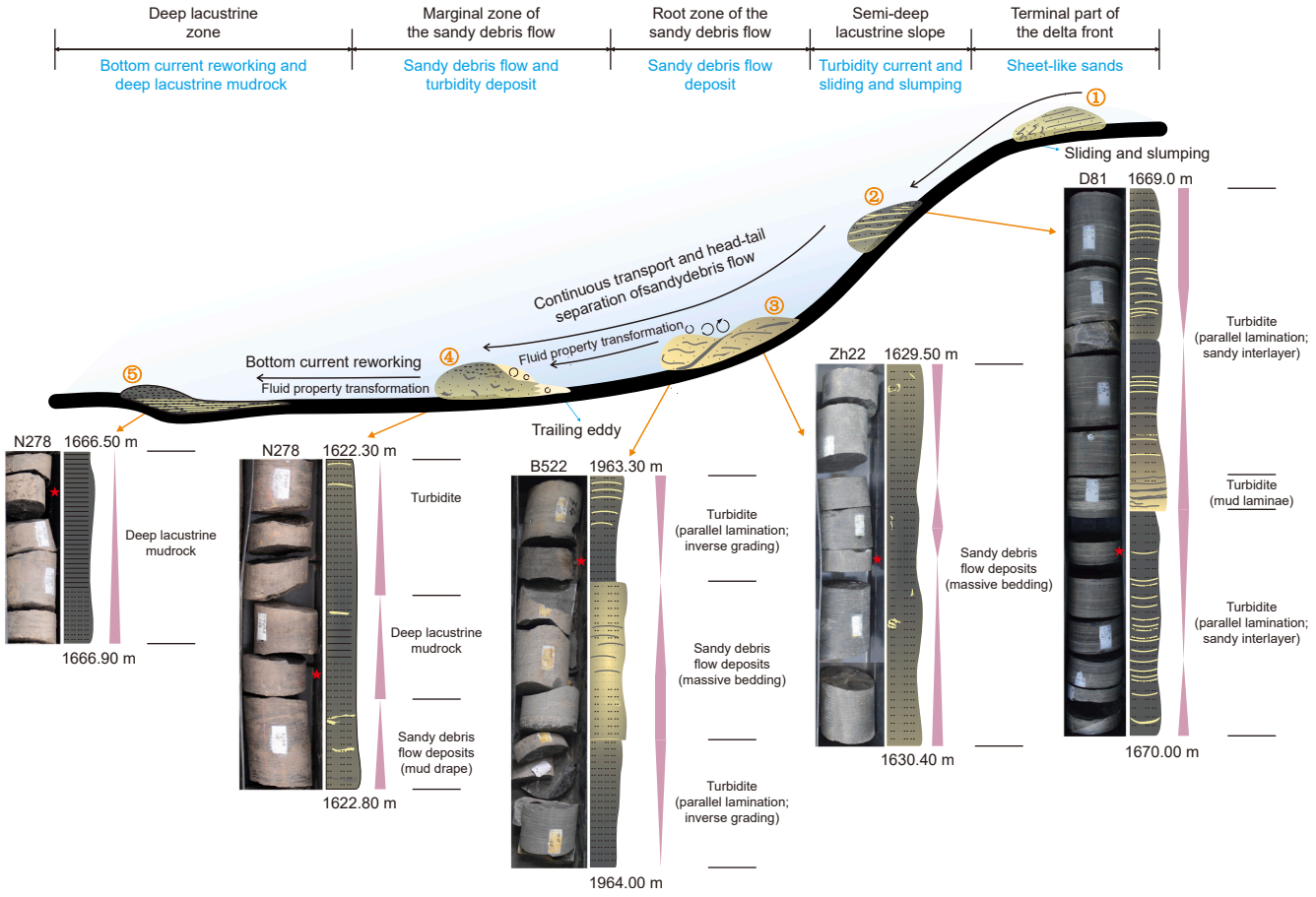

Fig. 11. Fine-grained gravity flow sedimentation model and core-based sedimentary sketches from different wells of the Ch-7 member, the Ordos Basin. Modified after Zhang et al. (2021).

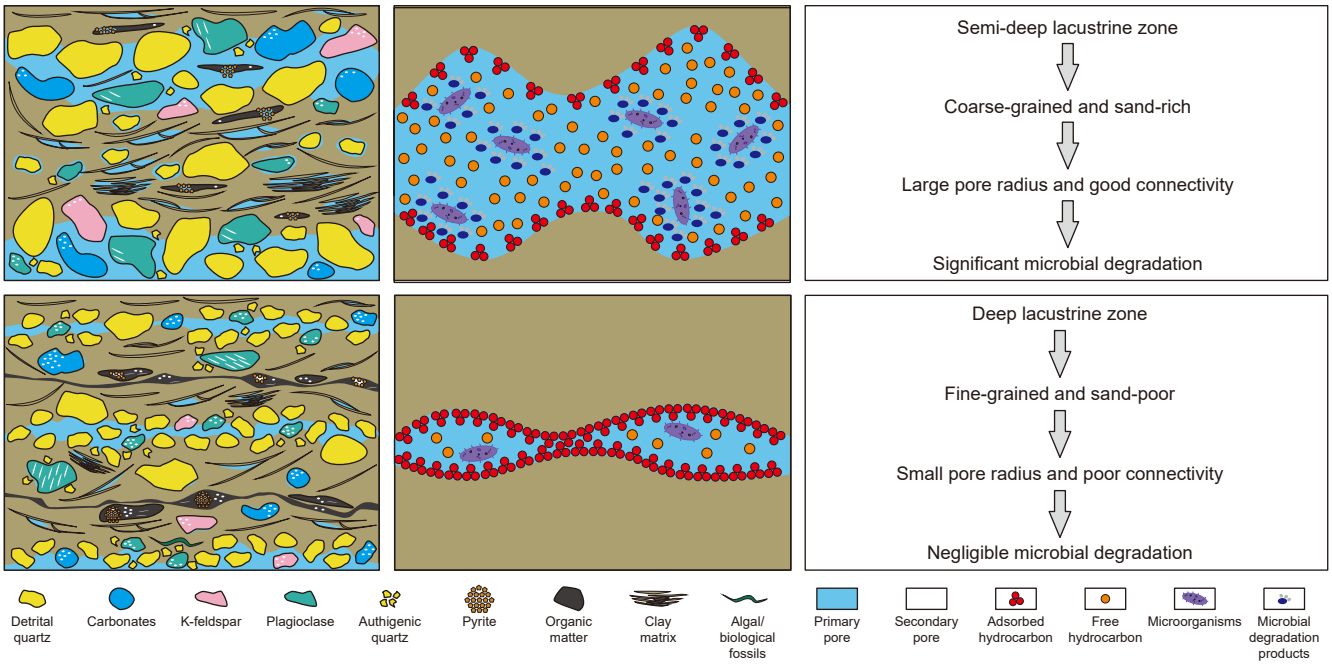

Fig. 12. Microbial degradation across different sedimentary facies in the Ch-7 shale series.

toward the lake center. From D81, Zh22, and B522 to N278, sedimentary facies changed from delta-front to semi-deep and deep-lake settings, accompanied by a progressive decline in sandy content and grain size, reflecting weakened hydrodynamic energy and nutrient input.

Overall, the Ch-7 shale contains abundant sandy laminae and interlayers that introduced terrestrial microorganisms and nutrients, providing the material basis for microbial hydrocarbon oxidation. Potential electron acceptors for anaerobic microbial oxidation in the Ordos Basin include sulfate (SO_4^{2-}), nitrate (NO_3^-), and ferric iron (Fe^{3+}), which may be supplied by formation waters or iron-bearing minerals in the shale matrix. With increasing water depth, the sandy laminae become thinner and finer, reducing pore connectivity and restricting microbial transport and nutrient diffusion. Concurrently, the pore system evolves from mixed adsorbed-free hydrocarbons to predominantly adsorbed hydrocarbons. At nanometer-scale pore throats, nanoconfinement effects further modify fluid dielectric properties, thereby limiting electron transfer between microorganisms and hydrocarbons and suppressing oxidation efficiency (Renou et al., 2014; Chogani et al., 2025). In relatively shallower semi-deep lacustrine zones, moderate pore connectivity allows limited microbial degradation under favorable thermal conditions (~80 °C, <2000 m depth; Fig. 12), although overall oxidation intensity remains weak due to the tight nature of the mudrocks.

6. Conclusions

This study highlights the anaerobic microbial oxidation of hydrocarbons within the Ch-7 shale of the Ordos Basin, providing new insights into the biogeochemical processes operating in low-permeability shale reservoirs. Three main conclusions have been drawn.

(1) The thermally desorbed hydrocarbons within shale samples can be divided into two categories, three samples exhibit microbial degradation characteristics with $\Delta_{C\text{-}T}$ values ranging from 3.9‰ to 7.9‰ $\delta^{13}C_{central}$ values ranging from −27.2‰ to −22.9‰, and $\delta^{13}C_{terminal}$ values ranging from −31.1‰ to −30.5‰, which are significantly higher than those of shale samples without microbial degradation.

(2) Microbial oxidation preferentially enriches the $\delta^{13}C_{central}$ values of propane, while the $\delta^{13}C_{terminal}$ values remains largely unchanged, preserving its original isotopic signature. This distinct intramolecular isotopic pattern serves as a sensitive and reliable indicator of microbial degradation in shale reservoirs.

(3) Microbial oxidation in the Ch-7 shale is controlled by the sand supply from different sedimentary facies within the shale series. As the depositional environment shifts to deeper lacustrine settings, reduced pore connectivity, finer grain size, and enhanced nanoconfinement effects limit nutrient transport and microbial mobility, resulting in generally low oxidation potential.

CRediT authorship contribution statement

Rui-Liang Guo: Writing – original draft. **Juske Horita:** Writing – review & editing. **Ji-Hong Li:** Funding acquisition. **Yun-Chao Hou:** Resources. **Jun-Lin Chen:** Visualization. **Peng Liu:** Writing – review & editing, Formal analysis, Conceptualization.

Declaration of competing interest

The authors declare that they have no known competing financial interests or personal relationships that could have appeared to influence the work reported in this paper.

Acknowledgement

This study was supported by the National Science and Technology Major Project of China (Oil & Gas Major Project) (Grant No. 2025ZD1400200, Grantee: Ruiliang Guo) and U.S. Department of

Energy Geosciences program (Grant No. DE-SC0016271, Grantee: Juske Horita).

References

Chogani, A., King, H.E., Tutolo, B., Zivkovic, A., Plümper, O., 2025. Geochemistry of lithospheric aqueous fluids modified by nanoconfinement. Nat. Geosci. 18, 191–196. https://doi.org/10.1038/s41561-024-01629-5.

Dang, C.C., Jin, Y.Z., Tan, X., Nie, W.B., Lu, Y., Liu, B.F., Xing, D.F., Ren, N.Q., Xie, G.J., 2024. Nitrite-driven anaerobic ethane oxidation. Environ. Sci. Ecotechnol. 21, 100438. https://doi.org/10.1016/j.ese.2024.100438.

Ding, Y.N., Li, B.B., Li, J.H., Duan, S.L., Song, H.S., Zeng, X.Y., 2023. A study of gas transport mechanisms in shale's confined nanopores: examining irregularity, adsorption effects, and stresses. Phys. Fluids 35 (12), Article 126108. https://doi.org/10.1063/5.0172862.

Gao, L., Brassell, S.C., Mastalerz, M., Schimmelmann, A., 2013. Microbial degradation of sedimentary organic matter associated with shale gas and coalbed methane in eastern Illinois Basin (Indiana), USA. Int. J. Coal Geol. 107, 152–164. https://doi.org/10.1016/j.coal.2012.09.002.

Gilbert, A., Yamada, K., Suda, K., Ueno, Y., Yoshida, N., 2016. Measurement of position-specific ^{13}C isotopic composition of propane at the nanomole level. Geochem. Cosmochim. Acta 177, 205–216. https://doi.org/10.1016/j.gca.2016.01.017.

Gilbert, A., Lollar, B.S., Musat, F., Giunta, T., Chen, S.C., Kajimoto, Y., Yamada, K., Boreham, C.J., Yoshida, N., Ueno, Y., 2019. Intramolecular isotopic evidence for bacterial oxidation of propane in subsurface natural gas reservoirs. Proc. Natl. Acad. Sci. USA 116 (14), 6653–6658. https://doi.org/10.1073/pnas.1817784116.

Gittins, D.A., Bhatnagar, S., Huberta, C.R.J., 2023. Environmental selection and biogeography shape the microbiome of subsurface petroleum reservoirs. mSystems 8 (2), Article e00884-22. https://doi.org/10.1128/msystems.00884-22.

Guo, R., Yang, W., Deng, X., Shi, S., Li, S., Qiu, J., Zhang, J., Chen, J., Hao, L., Ma, X., Ma, D., Liu, P., 2024. Dynamic coupling between cementation and porosity evolution of the Chang 8 tight sandstone reservoir, Ordos Basin: insights from in-situ microanalysis. Mar. Petrol. Geol. 164, 106840. https://doi.org/10.1016/j.marpetgeo.2024.106840.

Guo, R.L., Zhou, X.P., Lei, X.L., Liu, S.H., Chen, J.L., Liu, P., 2025a. Intramolecular isotopic distributions of associated propane in shale oil determined by an improved GC-Pyrolysis-GC-IRMS approach: insights into influence of kerogen structures on enrichment of hydrocarbon deposits. J. Anal. Appl. Pyrolysis 188, Article 107023. https://doi.org/10.1016/j.jaap.2025.107023.

Guo, R.L., Liang, X.W., Zhou, X.P., Fan, Z.Q., Zhao, J.Z., Bai, Y.B., Wu, W.T., Cao, L., Liu, P., 2025b. Effect of extractable organic matter on nanopore structure and heterogeneity in Triassic Yanchang lacustrine shale of the Ordos basin, China. J. Asian Earth Sci. 287, Article 106577. https://doi.org/10.1016/j.jseaes.2025.106577.

Guo, R.L., Li, S.X., Zhou, X.P., Guo, Q.H., Li, S.T., Chen, J.L., Zhang, J.Q., Hao, L.W., Ma, X.F., Qiu, J.L., Wang, Y., Liu, P., 2022. Multi-isothermal stage pyrolysis of the Chang 7(3)Shale OilReservoirs, ordos Basin: implications for oil occurrence states and in situ conversion exploitation. ACS Earth Space Chem. 6 (4), 1143–1162. https://doi.org/10.1021/acsearthspacechem.2c00057.

Head, I.M., Jones, D.M., Larter, S.R., 2003. Biological activity in the deep subsurface and the origin of heavy oil. Nature 426 (6964), 344–352. https://doi.org/10.1038/nature02134.

Heider, J., Spormann, A.M., Beller, H.R., Widdel, F., 1998. Anaerobic bacterial metabolism of hydrocarbons. FEMS Microbiol. Rev. 22 (5), 459–473. https://doi.org/10.1111/j.1574-6976.1998.tb00381.x.

Jaekel, U., Vogt, C., Fischer, A., Richnow, H.H., Musat, F., 2014. Carbon and hydrogen stable isotope fractionation associated with the anaerobic degradation of propane and butane by marine sulfate-reducing bacteria. Environ. Microbiol. 16 (1), 130–140. https://doi.org/10.1111/1462-2920.12251.

Jaekel, U., Musat, N., Adam, B., Kuypers, M., Grundmann, O., Musat, F., 2013. Anaerobic degradation of propane and butane by sulfate-reducing bacteria enriched from marine hydrocarbon cold seeps. ISME J. 7 (5), 885–895. https://doi.org/10.1038/ismej.2012.159.

Jiang, L., Worden, R.H., Cai, C.F., 2014. Thermochemical sulfate reduction and fluid evolution of the Lower Triassic Feixianguan Formation sour gas reservoirs, northeast Sichuan Basin, China. AAPG Bull. 98 (5), 947–973. https://doi.org/10.1306/10171312220.

Karnachuk, O.V., Lukina, A.P., Kadnikov, V.V., Sherbakova, V.A., Beletsky, A.V., Mardanov, A.V., Ravin, N.V., 2021. Targeted isolation based on metagenome-assembled genomes reveals a phylogenetically distinct group of thermophilic spirochetes from deep biosphere. Environ. Microbiol. 23 (7), 3585–3598. https://doi.org/10.1111/1462-2920.15218.

Kim, J.H., Martini, A.M., Ono, S., Lalk, E., Ferguson, G., McIntosh, J.C., 2023. Clumped and conventional isotopes of natural gas reveal basin burial, denudation, and biodegradation history. Geochem. Cosmochim. Acta 361, 133–151. https://doi.org/10.1016/j.gca.2023.10.017.

Kniemeyer, O., Musat, F., Sievert, S.M., Knittel, K., Wilkes, H., Blumenberg, M., Michaelis, W., Classen, A., Bolm, C., Joye, S.B., Widdel, F., 2007. Anaerobic oxidation of short-chain hydrocarbons by marine sulphate-reducing bacteria. Nature 449 (7164), 898. https://doi.org/10.1038/nature06200.

Li, X.Q., Horita, J., 2022. Kinetic and equilibrium reactions on natural and laboratory generation of thermogenic gases from Type II marine shale. Geochem. Cosmochim. Acta 333, 263–283. https://doi.org/10.1016/j.gca.2022.07.020.

Liu, C.J., McGovern, G.P., Liu, P., Zhao, H., Horita, J., 2018. Position-specific carbon and hydrogen isotopic compositions of propane from natural gases with quantitative NMR. Chem. Geol. 491, 14–26. https://doi.org/10.1016/j.chemgeo.2018.05.011.

Liu, C.J., Liu, P., Wang, X.F., Li, X.Q., Horita, J., 2023a. Establishing the accuracy of position-specific carbon isotope analysis of propane by GC-pyrolysis-GC-IRMS. Rapid Commun. Mass Spectrom. 37 (9), Article e9494. https://doi.org/10.1002/rcm.9494.

Liu, P., Wang, X.F., Liu, C.J., Liu, W.H., 2023b. Kinetic isotope effect and reaction pathways of thermogenic propane generation at early maturation stage: insights from position-specific carbon isotope distribution. Mar. Petrol. Geol. 153, Article 106252. https://doi.org/10.1016/j.marpetgeo.2023.106252.

Liu, P., Wang, X.F., Lin, Y., Liu, C.J., Li, X.F., Liu, W.H., 2020. Chemical and carbon isotope fractionations of alkane gases desorbed from confined systems and the application toward shale gas reservoir. Mar. Petrol. Geol. 113, Article 104103. https://doi.org/10.1016/j.marpetgeo.2019.104103.

Liu, P., Wang, X.F., Liu, C.J., Lin, Y., Guo, R.L., Liu, W.H., 2024. Intramolecular carbon isotopic rollover in propane from natural gas reservoirs of the Santanghu Basin: insights into chemical structure of kerogen. Org. Geochem. 188, Article 104740. https://doi.org/10.1016/j.orggeochem.2024.104740.

Liu, P., Wang, X.F., Wang, J., Horita, J., Wang, Z.Y., Lin, Y., Guo, R.L., Li, F.Q., Liu, W.H., 2025. Deciphering origins of hydrocarbon deposits by means of intramolecular carbon isotopes of propane adsorbed on sediments. Pet. Sci. 22 (2), 546–556. https://doi.org/10.1016/j.petsci.2024.10.007.

Liu, P., Wang, X., Liu, H., Horita, J., Zhou, G., Bao, H., Lin, Y., Guo, R., Zhang, D., Liu, W., 2026. Intramolecular carbon isotopic fractionation of propane via thermochemical sulfate reduction (TSR) in natural gas reservoirs. Nat. Gas. Ind. B 13 (1), 1–8. https://doi.org/10.1016/j.ngib.2025.12.001.

Luo, X.R., Zhang, L.K., Lei, Y.H., 2020. Petroleum migration and accumulation: modeling and applications. AAPG Bull. 104 (11), 2247–2265. https://doi.org/10.1306/0422201618817104.

Lyu, Q., Fu, J., Luo, S., Li, S., Zhou, X., Pu, Y., Yan, H., 2022. Sedimentary characteristics and model of gravity flow channel-lobe complex in a depression lake basin:a case study of Chang 7 member of Triassic Yanchang Formation in Southwestern ordos Basin,NW China. Petrol. Explor. Dev. 49 (6), 1143–1156. https://doi.org/10.1016/S1876-3804(23)60352.

Martini, A.M., Walter, L.M., McIntosh, J.C., 2008. Identification of microbial and thermogenic gas components from Upper Devonian black shale cores, Illinois and Michigan basins. AAPG Bull. 92 (3), 327–339. https://doi.org/10.1306/10180706037.

McIntosh, J., Kim, J.H., Bailey, L., Osburn, M., Drake, H., Martini, A., Reiners, P., Stevenson, B., Ferguson, G., 2023. Burial and denudation alter microbial life at the bottom of the hypo-critical zone. G-cubed 24 (6), Article e2022GC010831. https://doi.org/10.1029/2022gc010831.

Meckenstock, R.U., von Netzer, F., Stumpp, C., Lueders, T., Himmelberg, A.M., Hertkorn, N., Schmitt-Kopplin, P., Harir, M., Hosein, R., Haque, S., Schulze-Makuch, D., 2014. Water droplets in oil are microhabitats for microbial life. Science 345 (6197), 673–676. https://doi.org/10.1126/science.1252215.

Meng, Q., Wang, X.F., Wang, X.Z., Shi, B.G., Luo, X.R., Zhang, L.X., Lei, Y.H., Jiang, C.F., Liu, P., 2017. Gas geochemical evidences for biodegradation of shale gases in the Upper Triassic Yanchang formation, Ordos Basin, China. Int. J. Coal Geol. 179, 139–152. https://doi.org/10.1016/j.coal.2017.05.018.

Pavlova, O.N., Izosimova, O.N., Chernitsyna, S.M., Ivanov, V.G., Pogodaeva, T.V., Khabuev, A.V., Gorshkov, A.G., Zemskaya, T.I., 2022. Anaerobic oxidation of petroleum hydrocarbons in enrichment cultures from sediments of the Gorevoy Utes natural oil seep under methanogenic and sulfate-reducing conditions. Microb. Ecol. 83 (4), 899–915. https://doi.org/10.1007/s00248-021-01802-y.

Renou, R., Szymczyk, A., Ghoufi, A., 2014. Influence of the pore length on the properties of water confined in a silica nanopore. Mol. Phys. 112 (17), 2275–2281. https://doi.org/10.1080/00268976.2014.892167.

Shen, W.J., Zheng, L.G., Oldenburg, C.M., Cihan, A., Wan, J.M., Tokunaga, T.K., 2018. Methane diffusion and adsorption in shale rocks: a numerical study using the dusty gas model in TOUGH2/EOS7C-ECBM. Transport Porous Media 123 (3), 521–531. https://doi.org/10.1007/s11242-017-0985-y.

Sierra-Garcia, I.N., Belgini, D.R.B., Torres-Ballesteros, A., Paez-Espino, D., Capilla, R., Neto, E.V.S., Gray, N., de Oliveira, V.M., 2020. In depth metagenomic analysis in contrasting oil wells reveals syntrophic bacterial and archaeal associations for oil biodegradation in petroleum reservoirs. Sci. Total Environ. 715, Article 136646. https://doi.org/10.1016/j.scitotenv.2020.136646.

Song, D., Liu, P., Horita, J., Zhang, J., Wang, X., Tuo, J., 2025. Position-specific carbon isotope compositions of propane as a novel proxy for tracing sealing integrity of shale systems. GSA Bulletin. https://doi.org/10.1130/B38616.1%JGSABulletin.

Suarez-Zuluaga, D.A., Jan, W.J., Timmers, P.H.A., Buisman, C.J.N., 2015. High rates of anaerobic oxidation of methane, ethane and propane coupled to thiosulphate reduction. Environ. Sci. Pollut. Control Ser. 22 (5), 3697–3704. https://doi.org/10.1007/s11356-014-3606-0.

Wang, F., Chen, R., Yu, W., Tian, J.C., Liang, X.W., Tan, X.F., Gong, L., 2021. Characteristics of lacustrine deepwater fine-grained lithofacies and source-reservoir combination of tight oil in the Triassic chang 7 member in Ordos Basin, China. J. Petrol. Sci. Eng. 202, Article 108429. https://doi.org/10.1016/j.petrol.2021.108429.

Wang, X., Liu, P., Liu, W., Liu, C., Lin, Y., Zhang, D., 2024. Intramolecular carbon isotope of propane from coal-derived gas reservoirs of sedimentary basins: implications for source, generation and post-generation of hydrocarbons. Geosci. Front. 15 (4). https://doi.org/10.1016/j.gsf.2024.101806.

Wang, X.F., Liu, P., Meng, Q., Weniger, P., Liu, W.H., 2022. Physical selectivity on isotopologues of gaseous alkanes by shale pore network: evidence from dynamic adsorption process of natural gas. J. Nat. Gas Sci. Eng. 97, Article 104252. https://doi.org/10.1016/j.jngse.2021.104252.

Wang, X.T., Li, X.Z., Yu, L., Huang, L.X., Xiu, J.L., Lin, W., Zhang, Y.M., 2019. Characterizing the microbiome in petroleum reservoir flooded by different water sources. Sci. Total Environ. 653, 872–885. https://doi.org/10.1016/j.scitotenv.2018.10.410.

Whiticar, M.J., 1996. Stable isotope geochemistry of coals, humic kerogens and related natural gases. Int. J. Coal Geol. 32 (1-4), 191–215. https://doi.org/10.1016/s0166-5162(96)00042-0.

Whiticar, M.J., Faber, E., 1986. Methane oxidation in sediment and water column environments - isotope evidence. Org. Geochem. 10 (4-6), 759–768. https://doi.org/10.1016/s0146-6380(86)80013-4.

Widdel, F., Rabus, R., 2001. Anaerobic biodegradation of saturated and aromatic hydrocarbons. Curr. Opin. Biotechnol. 12 (3), 259–276. https://doi.org/10.1016/s0958-1669(00)00209-3.

Yao, J., Song, W.H., Wang, D.Y., Sun, H., Li, Y., 2019. Multi-scale pore network modelling of fluid mass transfer in nano-micro porous media. Int. J. Heat Mass Tran. 141, 156–167. https://doi.org/10.1016/j.ijheatmasstransfer.2019.06.077.

Zeng, K.C., Jiang, P.X., Xu, R.A., 2023. Restricted CO_2/CH_4 diffusion in nanopores: a quantitative framework to characterize nanoconfinement effect of shale organic pore. Int. J. Heat Mass Tran. 210, Article 124178. https://doi.org/10.1016/j.ijheatmasstransfer.2023.124178.

Zengler, K., Richnow, H.H., Rosselló-Mora, R., Michaelis, W., Widdel, F., 1999. Methane formation from long-chain alkanes by anaerobic microorganisms. Nature 401 (6750), 266–269. https://doi.org/10.1038/45777.

Zhang, J., Li, S., Zhou, X., Liu, J., Guo, R., Chen, J., Li, S., 2021. Gravity flow deposits in the distal lacustrine basin of the 7th reservoir group of Yanchang formation and deepwater oil and gas exploration in Ordos Basin: a case study of Chang 73 sublayer of Chengye horizontal well region. Acta Pet. Sin. 42 (5), 570–587.

Zhang, T.W., Sun, X., Milliken, K.L., Ruppel, S.C., Enriquez, D., 2017. Empirical relationship between gas composition and thermal maturity in Eagle Ford Shale, south Texas. AAPG Bull. 101 (8), 1277–1307. https://doi.org/10.1306/09221615209.

Zhao, H., Liu, C.J., Larson, T.E., McGovern, G.P., Horita, J., 2020. Bulk and position-specific isotope geochemistry of natural gases from the Late Cretaceous Eagle Ford Shale, south Texas. Mar. Petrol. Geol. 122, Article 104659. https://doi.org/10.1016/j.marpetgeo.2020.104659.